Insulating Polymers for Enhancing the Efficiency of Non-Fullerene Organic Solar Cells

Meng Wang, Shenghua Liu, Peng You, Naixiang Wang, Guanqi Tang, Qian Miao and Feng YAN*

Dr. M. Wang, S. H. Liu, P. You, N. X. Wang, G. Q. Tang, Prof. F. Yan
Department of Applied Physics, The Hong Kong Polytechnic University, Hung Hom, Kowloon, Hong Kong, P. R. China
E-mail: apafyan@polyu.edu.hk

Prof. M. Qian
Department of Chemistry, The Chinese University of Hong Kong, Shatin, New Territories, Hong Kong, P. R. China

A series of insulating polymers are used as additives in non-fullerene organic solar cells (OSCs) for the first time. A significant relative power conversion efficiency (PCE) enhancement of up to 16% is observed with an introduction of polystyrene for only 5.0 wt.% into the active layer of OSCs. Other insulating polymers possessing linear non-conjugated backbones with different side chains were also incorporated into OSCs and the resultant PCE enhancement decreases with the decrease of the side chain size. Another important issue we noticed is the glass transition temperature of the polymer additive. When the glass transition temperature is higher than the thermal annealing temperature of the active layer, the polymer additive plays a negative effect on the device performance and the device efficiency decreases monotonically with the increase of addition amount. So the effect of the insulating polymer additives in non-fullerene OSCs can be attributed to the reconstruction of the active layer films, which increases the crystallinity, carrier mobility and carrier lifetime of the organic semiconductors in the bulk heterojunction of the devices. This work provides a guideline for the selection of polymer additives in OSCs besides the consideration on the optoelectronic property of the additives.

1. Introduction

OSCs have attracted considerable attention during the past two decades owing to the high efficiency, light weight, low cost, mechanical flexibility, solution processability of the devices.[1-5] Among the bulk heterojunction (BHJ) OSCs, both the donor and acceptor materials are critical to the PCEs of the devices. Fullerene derivatives are the most widely used electron acceptor materials since the first report by Wudl *et al.* in 1995.[6] Recently, non-fullerene small-molecule acceptors have been developed as alternatives to fullerene derivatives, offering advantages of good stability, easily tunable energy levels, and broadband absorption range.[7-19] In 2015, Zhan *et al.* synthesized a planar non-fullerene electron acceptor 3,9-bis(2-methylene-(3-(1,1-dicyanomethylene)-indanone))-5,5,11,11-tetrakis(4-hexylphenyl)-dithieno[2,3-d:2',3'-d']-s-indaceno[1,2-b:5,6-b']dithiophene (ITIC) and used it in OSCs with a record PCE for non-fullerene OSCs at that moment.[20] In 2016, Hou *et al.* reported a new type of high-efficiency non-fullerene OSCs based on poly[(2,6-(4,8-bis(5-(2-ethylhexyl)thiophen-2-yl)-benzo[1,2-b:4,5-b']dithiophene))-alt-(5,5-(1',3'-di-2-thienyl-5',7'-bis(2-ethylhexyl)benzo[1',2'-c:4',5'-c']dithiophene-4,8-dione))] (PBDB-T):ITIC with PCE up to 11.2% and excellent thermal stability.[21] After fluorination of the organic semiconductors, they further enhanced the PCE of OSCs up to over 13% based on PBDB-T-SF:IT-4F.[22] Nowadays, a new acceptor material Y6 was synthesized by Zou *et al.* exhibiting a high charge carrier mobilities and a broad absorption range from 400 nm to 950 nm. As a result, a new PCE record of 15.7% has been realized when they incorporated Y6 with PM6 in OSCs.[23]

Notably, PCEs of OSCs are still lower than those of inorganic solar cells because of the low carrier mobilities and short exciton diffusion lengths in organic semiconductors.[24] One feasible approach is to introduce additives such as plasmonic nanoparticles[25-28], 2-dimensional materials[29-34] and high mobility polymers[35] in OSCs to enhance light absorption as well as carrier transportation in the devices. We have demonstrated the successful additions of black phosphorus quantum dots, Au/Ag core-shell nanocuboids and high-mobility conjugated polymers into OSCs based on PTB7:PC$_{71}$BM or PBDTTT-EFT:PC$_{71}$BM[25, 29, 35-36], and the

PCEs of the devices were all improved relatively for over 10%. Besides the enhanced light absorption and carrier transfer in BHJ active layers induced by the additives, the morphological change of BHJ can be another critical issue to the device performance. In this regard, the introduction of insulating polymers in OSCs as additives can make clear this issue because the added polymers have no direct contribution to the carrier transfer and light absorption of the active layers. Some insulating polymers, such as polystyrene (PS) and poly (4-vinylpyridine) (P4VP), have been introduced in fullerene-based OSCs to improve the device performance.[37-39] For example, Bazan *et al.* reported that PS could increase the thickness and absorbance of the active layer of fullerene –based OSCs.[37-38] However, the introduction of insulating polymer additives into the non-fullerene OSCs has not been reported.

In this paper, we introduced PS and a series of non-conjugated insulting polymers such as polyethylene glycol (PEG), polydimethylsiloxane (PDMS), polymethylmethacrylate (PMMA), polyvinyl pyrrolidone (PVP), and polyvinyl carbazole (PVK) as additives into the active layers of non-fullerene OSCs based on PBDB-T:ITIC. These insulators possess a linear non-conjugated backbone with different side chains. With the introduction of PS for 5.0 wt.%, OSCs with PCEs up to 11.58% are achieved, which are about 13% enhancement relative to those of control devices. Other insulating polymers, including PEG, PDMS, PMMA, and PVP, also lead to PCE enhancements at optimum addition levels. The significant enhancement of the device performance can be attributed to the improved polymer crystallinity, carrier mobility and lifetime induced by the polymer additives. Interestingly, we find that the thermal annealing temperature of the active layer should be higher than the glass transition temperatures (T_g) of the additives, which is important to the reconstruction of the active layer morphology for better device performance. This work provides a guideline for the selection of polymer additives in OSCs besides the consideration on the optoelectronic property of the additives.
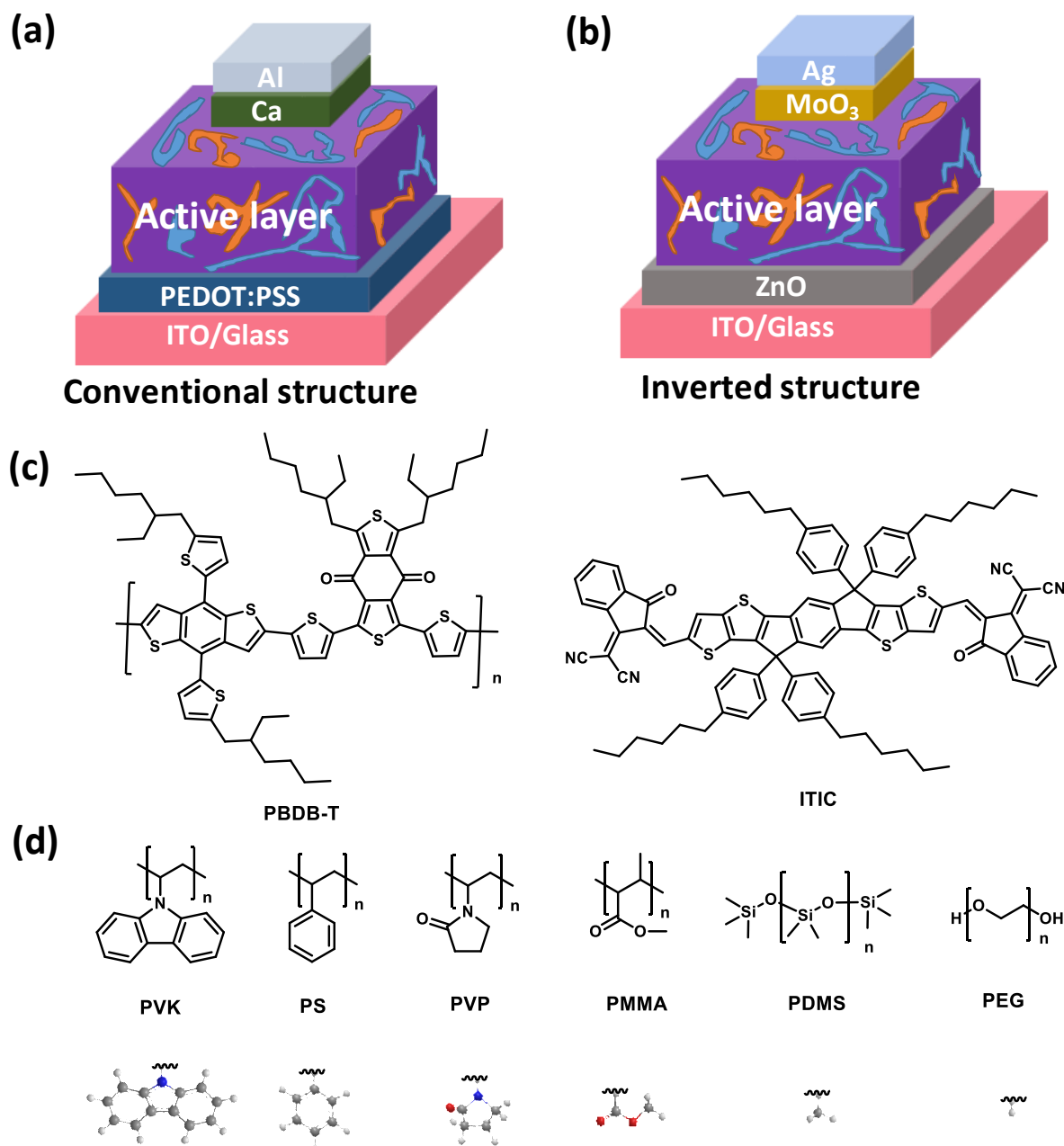
Figure 1. The structures of (a) conventional and (b) inverted OSCs based on PBDB-T:ITIC. (c) The molecular structures of PBDB-T, and ITIC used in the experiments. (d) The molecular structures and 3-dimentional structures of the biggest side chain per repeating unit of PVK, PS, PVP, PMMA, PDMS, PEG used in the experiments.

2. Results and Discussion

As shown in **Figure** 1a and 1b, OSCs based on PBDB-T:ITIC with polymer additives were fabricated with both conventional (ITO/PEDOT:PSS/active layer/Ca/Al) and inverted

architectures (ITO/ZnO/active layer/MoO$_3$/Ag). The molecular structures of the insulating polymer additives, including PVK, PS, PVP, PMMA, PDMS, PEG, and the semiconductors of PBDB-T and ITIC are shown in Figure 1c and 1d. All of these polymers can be dissolved in chlorobenzene, which is the solvent for the preparation of the active layers of OSCs.
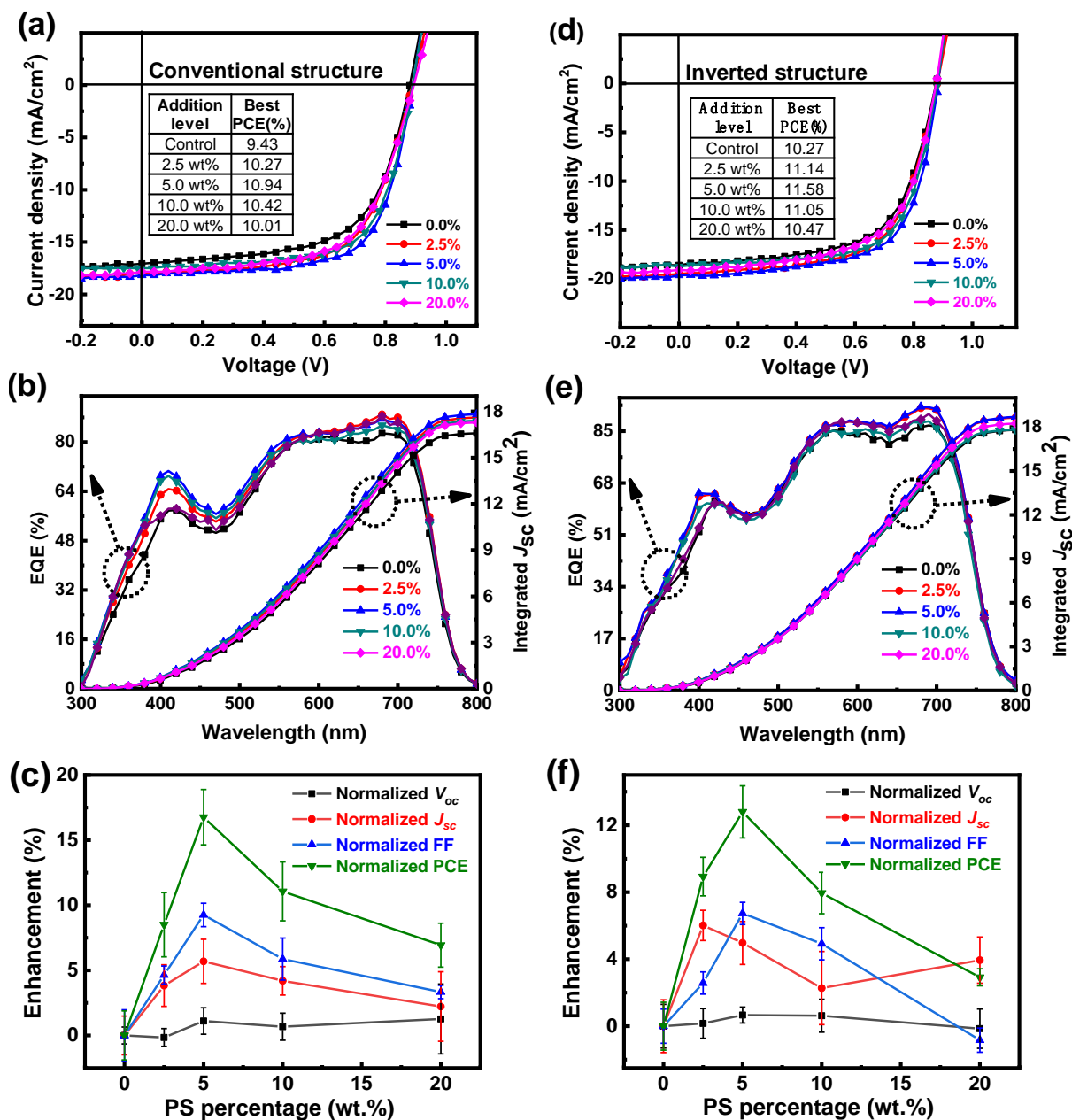
Figure 2. (a) *J–V* characteristics, (b) EQE, and (c) performance enhancement of the best conventional OSCs with various percentages of PS. (d) *J–V* characteristics, (e) EQE, and (f) performance enhancement of the best inverted OSCs with different percentages of PS.

PS was firstly added into the active layers of non-fullerene OSCs with weight percentages relative to PBDB-T of 2.5 wt.%, 5.0 wt.%, 10.0 wt.%, and 20.0 wt.%. The control devices based on PBDB-T:ITIC without PS were also prepared. Current density *versus* bias voltage (*J–V*) curves of the OSCs with the conventional structure are shown in Figure 2a. Compared with the control devices, the PCEs of the OSCs were substantially improved with the addition of PS. The maximum relative PCE enhancement is 16.7% when the addition level is 5.0 wt.%. However, further addition of PS for more than 5.0 wt.% inversely decreases the PCEs of the devices. The detailed photovoltaic parameters for different addition levels are summarized in Table 1.

Table 1. Photovoltaic properties of OSCs based on PBDB-T:PS:ITIC blends

Device structure	PS ratio[a] (wt.%)	V_{oc} (V)	J_{sc} (mA/cm^2)	FF (%)	PCE (%)	Enhancement[b] (%)
	0.0	0.88	17.07	62.75	9.43 (9.15±0.28)	0
	2.5	0.89	18.06	64.03	10.27 (9.93±0.35)	8.52±3.83
Conventional device	5.0	0.89	18.14	67.70	10.94 (10.68±0.26)	16.72±2.84
	10.0	0.89	17.51	66.98	10.42 (10.15±0.27)	10.93±2.95
	20.0	0.89	17.84	62.98	10.01 (9.78±0.23)	6.89±2.51
	0.0	0.88	18.62	62.89	10.27 (10.12±0.15)	0
	2.5	0.88	19.51	64.83	11.14 (11.02±0.12)	8.89±1.19
Inverted device	5.0	0.88	19.64	67.00	11.58 (11.42±0.16)	12.85±1.58
	10.0	0.88	18.75	66.90	11.05 (10.92±0.13)	7.91±1.28
	20.0	0.88	19.09	62.40	10.47 (10.42±0.05)	2.96±0.49

[a] PS percentage was relative to the PBDB-T (w/w). [b] Enhancement was calculated according to the average PCE.

The best control device with conventional structure exhibited a PCE of 9.43%, an open circuit voltage (V_{OC}) of 0.88 V, a short circuit current density (J_{SC}) of 17.07 mA/cm^2, and a fill factor (FF) of 62.75%. When 2.5 wt.% PS was incorporated into the active layer, the best OSC showed an improved efficiency of 10.27% due to the simultaneous improvement in both J_{SC} (18.06 mA/cm^2) and FF (64.03%). Increasing the percentage of PS to 5.0 wt.% led to a higher

efficiency of 10.94%, a better J_{SC} of 18.14 mA/cm^2 and FF of 67.70%. However, an increase of PS percentage to 10.0 wt.% resulted in a decreased PCE of 10.42% due to the decrease of both J_{SC} (17.51 mA/cm^2) and FF (66.98%). Further addition of PS to 20.0 wt.% induced degradation of the device performance and a lower PCE of 10.01%.

Figure 2b shows external quantum efficiency (EQE) characteristics of the devices. All the EQE spectra cover a broad wavelength range from 300 to 800 nm. The EQE values in the whole wavelength region are enhanced by PS. The photocurrent densities calculated from the EQE spectra are consistent with the enhanced J_{SC} of the devices. The performance enhancement of the OSCs by different PS addition levels are summarized in Figure 2c.

Inverted OSCs were also fabricated to test the effect of PS on the device performance. The J–V characteristics, EQE, and PCE enhancements of inverted OSCs with various percentages of PS are plotted in Figure 2d, 2e, and 2f, respectively. The photovoltaic parameters of the inverted devices are also presented in Table 1. The best control device based on PBDB-T:ITIC exhibited a PCE of 10.27%, a V_{OC} of 0.88 V, a J_{SC} of 18.62 mA/cm^2, and a FF of 62.89%, which are comparable with the performance in the literature.[21] Encouragingly, the device with 5.0 wt.% PS showed the highest PCE of 11.58% and a relative enhancement of 13% over the control device. The increase of J_{SC} in the J-V curves is consistent with the EQE spectra presented in Figure 2e. Hence, an appropriate addition of PS in the active layers can significantly enhance the photovoltaic performance of OSCs with both conventional and inverted structures.

To investigate the effect of PS on the carrier recombination processes, OSCs were characterized by using an impedance analyzer (HP4294) in the dark (See Supporting Information, Figure S1). The carrier lifetimes of the devices with the conventional structure were calculated according to the Nyquist curves shown in Figure 3a.[40] It is reasonable to find the decrease of carrier lifetime with the increase of bias voltage owing to the increased carrier density at the heterojunction.[35] At the same bias voltage, the increase of the PS addition level to 5.0 wt.% lead to the increase of the carrier lifetimes in the active layer, which is favorable
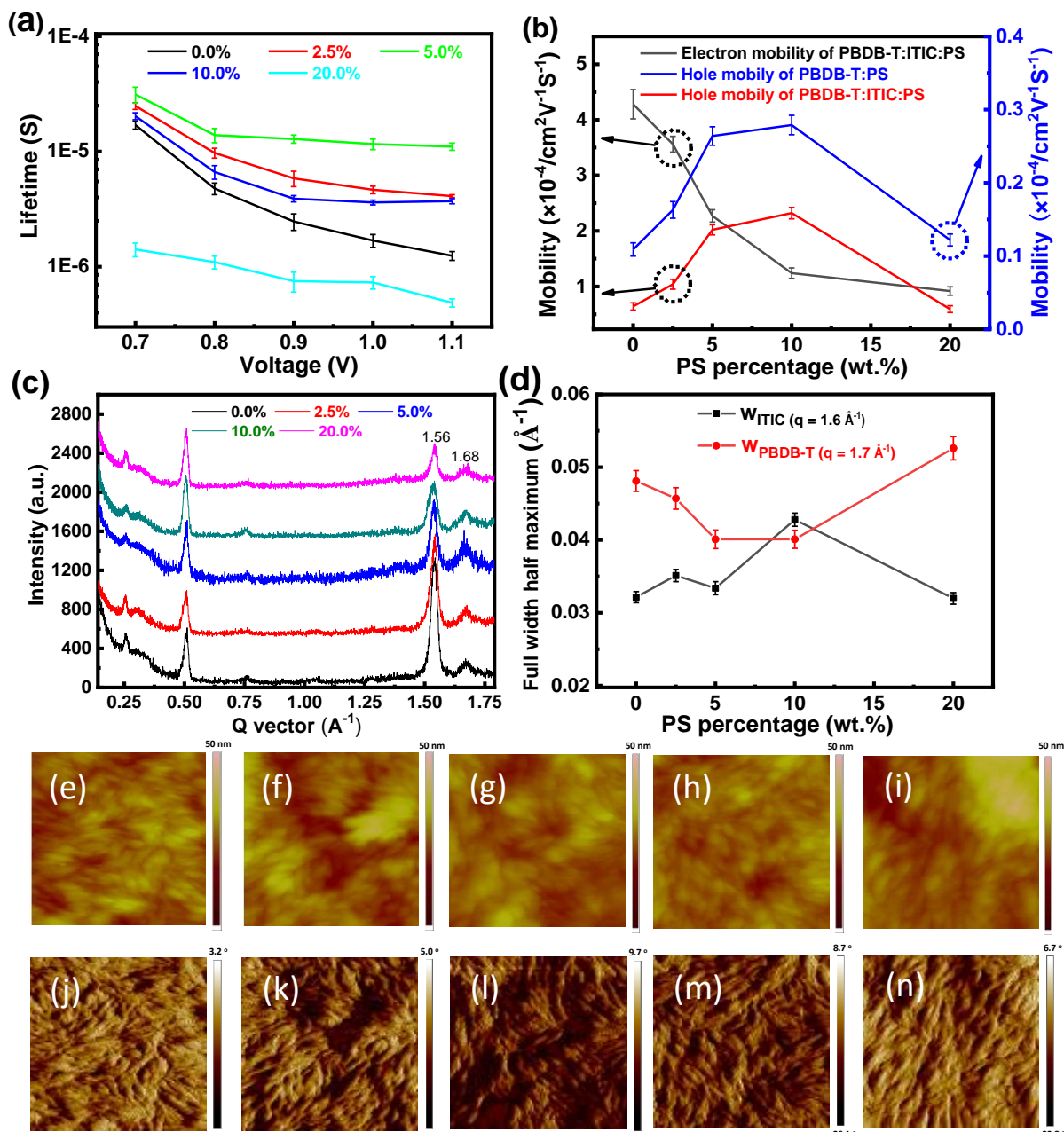
Figure 3. (a) Carrier lifetimes of conventional OSCs with various percentages of PS as a function of bias voltage. (b) Mobilities of active layers or polymer films with different percentages of PS. (c) The GIXD out-of-plane diffraction profiles of PBDB-T:PS:ITIC ternary films with different PS percentages. (d) Full width at half maximum of the diffraction peaks for different PS percentages in ternary films. Tapping mode AFM height (e-i) and phase (j-n) images of PBDB-T:ITIC films with 0.0%, 2.5% 5.0%, 10.0%, or 20.0% PS, respectively. All the AFM images are 500 nm × 500 nm.

for the photovoltaic performance of the devices. However, further increase of the PS addition levels inversely decreases the carrier lifetimes. These results are consistent with the PCE enhancement induced by PS at the same additive level. Similar effect was also observed in the inverted devices that shows the longest carrier lifetime at the optimum PS addition level of 5.0 wt.% (See supporting information, Figure S2).

Considering the carrier mobilities in the active layers of OSCs being critical to the device performance, we then characterized the effect of PS on the electron/hole mobilities in the devices by measuring the space charge-limited-current (SCLC) of the active layers. Hole only devices (ITO/PEDOT:PSS/active layer/Au) and electron only devices (ITO/ZnO/active layer/Al) were fabricated and tested in the dark.[35] The hole mobilities were extracted from $J^{0.5}$–V curves (see supporting information, Figure S3b) and plotted in Figure 3b. Notably, the hole mobility increases with the increase of PS addition level until 10.0 wt.% and then inversely decreases with the increase of PS addition.[41-43] To better understand the effect on hole mobility enhancement in OSCs, we characterized the hole mobilities of pure PBDB-T and its composites with PS for different percentages. The hole mobility in the pure PBDB-T film is higher than that in the active layer of OSCs due to the better crystallinity in the former. Similar enhancement of hole mobility induced by PS was also observed in the PBDB-T:PS composites, indicating that the crystallinity or orientation of PBDB-T is influenced by PS. It is reported that incorporating non-conjugated insulating PS into semiconductors leads to short-range intermolecular aggregation and higher mobility in organic field effect transistors (OFETs).[41-43] Normally, polarized surroundings inhibit carrier transportation in organic semiconductors. So the interface between a semiconductor and an insulating polymer may weaken the energetic disorder and activation energy in the semiconductor, resulting in a higher carrier mobility.[44] Electron mobilities were also obtained from the $J^{0.5}$–V curves (see supporting information, Figure S3a) and presented in Figure 3b. Notably, the electron mobility decreases with the increase of PS addition level. It is interesting to find that the electron and hole mobilities have

the similar values when the PS addition level is 5.0 wt.%. At this condition, the devices have balanced electron and hole transportation in the active layers, which is the major reason for the highest PCE obtained at this addition level.[35]

To clarify the effect of PS on the morphology of the active layer of OSCs, we characterized the organic thin films including ITIC, PBDB-T, PS and PBDB-T:PS:ITIC blend film by Grazing Incidence X-ray Diffraction (GIXD, Regaku 9 KW SmartLAB).[35] The GIXD out-of-plane diffraction profiles of pure organic films and BHJ films are shown in Figure S4 (Supporting Information) and Figure 3c, respectively. Compared to the GIXD curve of amorphous PS without any peak, both pure PBDB-T and ITIC films show obvious diffraction peaks.[45] The ITIC film shows two strong peaks at 0.52 and 1.56 Å^{-1}, corresponding to lamellar (edge-on) and π–π stacking (face-on) states, respectively. The PBDB-T film shows a low peak at 0.33 Å^{-1} for lamellar stacking and a broad peak at 1.68 Å^{-1} for π–π stacking. For the PBDB-T:PS:ITIC blend films shown in Figure 3c, two sharp peaks for ITIC were observed in all samples. With the increase of PS percentage, the peak intensity at 1.56 Å^{-1} corresponding to face-on state decreases, indicating that the crystallinity of ITIC was reduced by PS. For higher PS addition percentage, the electron mobility deceases with the increase of PS percentage.[45-46] For PBDB-T component, we find that the half width of the peak at 1.68 Å^{-1} decreases with the increase of PS percentage until 10.0 wt.% and then increases at higher percentages, indicating that 10.0 wt.% PS induced the best crystallinity of PBDB-T in the blend films. This result demonstrates that the highest hole mobility in the PBDB-T:PS:ITIC blend film obtained at 10.0 wt.% PS addition is reasonable.

The surface morphologies of PBDB-T:PS:ITIC blend films were characterized by atomic force microscopy (AFM), as shown in Figure 3e-n and Figure S5 (Supporting Information). Clear phase separation and fibrillar structures of PBDB-T were presented in all images. We assume that the "fiber" can serve as "expressway" for the fast transportation of charge carriers, which could further suppress the possibilities of carrier recombination and improve the

photovoltaic performance of the devices.[47] Without PS addition, the PBDB-T:ITIC film exhibits large domains and a root-mean-square (RMS) surface roughness of 5.10 nm. With the addition of small amount of PS, it is easy to find that the roughness values of the film decreased initially then increased with the increase of the PS percentage. 5 wt.% PS addition lead to the lowest film roughness as shown in figure S5 in the supporting Information, which is consistent with the PCE variation. Too much PS may destroy the properties of the semiconductor materials, prohibit the carrier transportation and decrease the performance of the OSCs. The experimental results indicate that PS has an impact on the morphology of the active layers of OSCs based on PBDB-T:ITIC.

In addition, we found that the addition of PS in the PBDB-T:ITIC blends increased the thickness of the active layer gradually. As depicted in Figure S6 in the supporting information, the thickness of the active layer increased from around 99 nm for the control device to 104 nm, 116 nm, 138 nm, and 157 nm when the additions of PS are 2.5 wt.%, 5.0 wt.%, 10.0 wt.% and 20.0 wt.%, respectively, which is one of the reasons for the improvement of J_{sc} of the PS - incorporated OSCs.

Notably, the glass transition temperature (T_g) of PS was measured to be 84 ^{o}C (Figure S7, Supporting Information). Therefore, during the thermal annealing process of the active layer, the flexible PS chains would not only change its configuration but also "redissolve" in the PBDB-T:ITIC blends to regulate the nonequilibrium morphology of the blend film.[48] PS may fill in the interspace and optimize the molecular packing to minimize the numbers of traps and defects in film, leading to an active layer with better crystallinity as well as higher carrier mobility and lifetime.[44] Therefore, PS can modify the donor and acceptor to effectively regulate the film morphology in nanoscale network. The active layer film with 5.0 wt.% PS addition shows well-aligned fibrillary nanostructure with the smallest domain size (~30 nm) and film roughness (3.25 nm), which is one of the reasons for the highest PCE obtained at the optimum conditions. We noticed that only little amount of PS can occupy the interspace

between PBDB-T and ITIC, resulting in the formation of bundle networks while too much PS may destroy the fiber and generate PS rich zone, inducing large aggregation with poor phase separation.
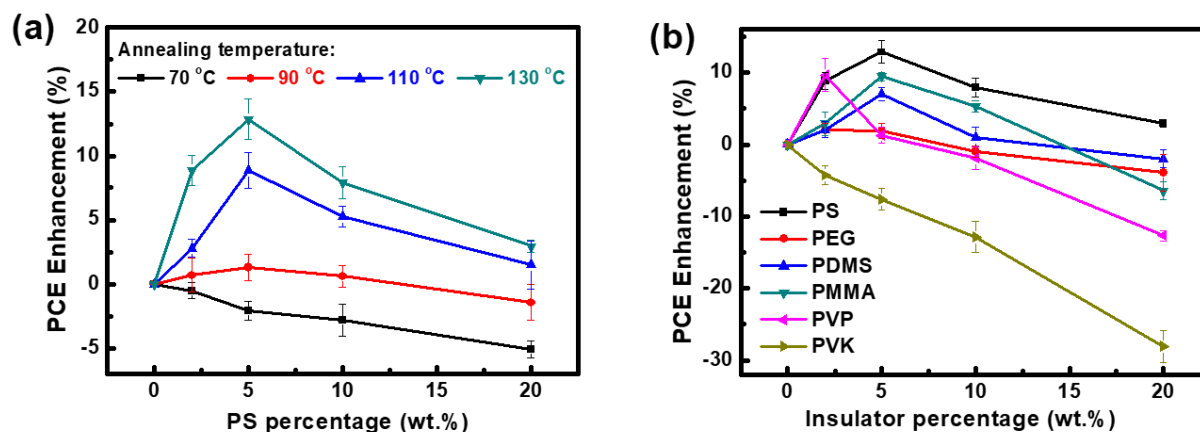
Figure 4. PCE enhancement of the inverted OSCs based on a) PBDB-T:PS:ITIC with various annealing temperatures and b) PBDB-T:ITIC with addition of different insulating polymers.

To make clear the temperature dependent reconstruction effect, PBDB-T:PS:ITIC -based OSCs with lower annealing temperatures of 70, 90, and 110 °C were also fabricated and characterized. The detailed parameters and PCE enhancement characteristics are shown in Table S1 (Supporting Information) and Figure 4a, respectively. For the annealing temperature of 70 °C, the PCEs of the devices decreased with the increase of PS percentage, indicating that PS has a negative effect on the device performance. When the annealing temperature was increased to 90 °C, the PCEs of the devices do not show obvious changes no matter when the PS addition percentage is varied from 0.0% to 20.0 wt.%. However, when the annealing temperature is much higher than T_g, the PS additive demonstrates prominent contributions to the photovoltaic performance of the OSCs, especially at 130 °C. We also incorporate PS into another typical PTB7:$PC_{71}BM$-based OSCs, and the corresponding performance is summarized in Table S2. However, the device performance decreases with the increase of PS percentage. Notably, the PTB7:$PC_{71}BM$-based devices were fabricated without thermal annealing. These

results suggest that the reconstruction effect of PS additive in the blend films only works well when the annealing temperature is higher than its T_g.

Other insulating polymers such as PEG, PDMS, PMMA, PVP, and PVK were also used as additives to fabricate OSCs. The photovoltaic parameters and PCE enhancement curves are shown in Table S3 (Supporting Information) and Figure 4b, respectively. For various percentages of PEG addition, no obvious influence on the device efficiencies can be observed. However, for addition of PDMS in the active layer, 5.0 wt.% of PDMS addition led to the maximum efficiency of 10.92%, which is about 7% enhancement relative to the control device. Moreover, the incorporation of 5.0 wt.% PMMA in the blend active layer resulted in an increased PCE of 11.14%. For PVP polymer, 2.5 wt.% PVP led to the highest PCE of 11.33% with 10% relative enhancement. On the other hand, the addition of PVK in the active layer led to negative effect on the PBDB-T:ITIC-based OSCs.

As shown in Figure S7 (Supporting Information), the T_g of PMMA, PVP, and PVK were measured to be 107, 75, and 226 °C, respectively. According to the literatures, the T_g of PEG[49] and PDMS[50] are 17 and -113 °C, respectively. As we demonstrated before, the reconstruction effect of the insulating additives on the active layer can work well when the annealing temperature of the blend film beyond the T_g of the additives. The T_g of PVK (226 °C) is higher than the annealing temperature of the active layer (130 °C). Therefore, the performance of the OSCs decreases with the increase of PVK percentage. More importantly, all the insulating polymers have the similar linear backbone with the increasing size of side chain for PEG, PDMS, PMMA, PVP, PS, and PVK in sequence. Notably, the PCEs of the OSCs increase with the increase of the side chain size of the polymer additives except PVK. A larger side chain could afford more sufficient volume and viscosity for the reconstruction of the active layer during thermal annealing at the temperature above T_g of the insulating polymer. This model also explains the reason why the addition of PEG cannot improve the PCE of OSCs since PEG has no side chain.

13

3. Conclusion

In summary, insulating polymer PS is used to improve the performance of non-fullerene OSCs based on PBDB-T:ITIC for the first time. After incorporating PS into the PBDB-T:ITIC active layer, 5.0 wt.% addition led to the highest PCE and 16% (13%) relative PCE enhancement for OSCs with a conventional (inverted) structure. The significant enhancement of the device performance was attributed to the fact that PS can reconstruct the active layer films to increase the polymer crystallinity as well as carrier mobility and lifetime of the devices. Other insulating polymers, including PEG, PDMS, PMMA, and PVP, can also improve the performance of OSCs with different levels and the relative enhancement increases with the increase of the side-chain size. In addition, the glass transition temperature of the polymer additive is a key factor to its influence on the OSC performance. When the annealing temperature of the BHJ layer is lower than the glass transition temperature of the polymer additive, the device performance can not be enhanced by the polymer. This work clearly indicates that, besides optoelectronic properties, the glass transition temperature and the side chain size of a polymer additive are also critical issues to the performance of OSCs.

4. Experimental Section

Materials: Reagents were purchased from Aldrich Inc., Adamas beta Ltd., Solarmer Materials Inc., Thermo Fisher Scientific Inc., International Laboratory USA Inc., or Heraeus Inc. and used without further purification unless otherwise stated.

Fabrication and Characterization of OSCs: The conventional OSCs were fabricated with the structure of indium tin oxide (ITO)/poly(3,4-ethylenedioxythiophene):poly(styrenesulfonate) (PEDOT:PSS)/active layer/Ca/Al. ITO glass was cleaned by ultrasonication sequentially in acetone, water, and isopropyl alcohol for 10 min each and then dried with nitrogen. After the ITO glass substrates were subjected to oxygen plasma for 6 min, PEDOT:PSS (Baytron PVPAI 4083) which had been filtered through a 0.45 µm filter was spin-coated on the ITO substrates at 3000 rpm for 60 s. Then the film-loaded substrates were dried at 150 ºC for 1 hour. PBDB-

T were blended with ITIC (1:1, w/w) in chlorobenzene and 0.5 vol% 1,8-diiodoctane (DIO) at a concentration of 20 mg/mL with or without different amounts (2.5% 5.0%, 10.0%, and 20.0%) of insulator additives relative to the weight of PBDB-T. After the mixtures were stirred overnight, the active layer was prepared by spin-coating and annealed at 130 ^{o}C for half an hour. After cooled to room temperature, methanol was spin-coated to remove the residual DIO. Eventually, the electron injection interlayer and negative electrode were prepared by thermally depositing about 20 nm calcium and 120 nm aluminum through a shadow mask under a high vacuum below 1×10^{-6} Torr, respectively. The active areas of the devices were fixed at 6 mm^2. The inverted OSCs were fabricated following the similar procedures of conventional structure, except the PEDOT:PSS, calcium, and aluminum were replaced by ~40 nm ZnO, 10 nm MoO$_3$ and 100 nm Ag, respectively.

Device Measurement: OSCs were encapsulated in glove box and measured by a Keithley 2400 source measurement unit under AM 1.5 G irradiation (100 mW/cm^2) from an Oriel sol3A simulator (Newport 91160, 300 W) which had been precisely calibrated with a National Renewable Energy Laboratory (NREL)-certified silicon reference cell. The EQE spectra were performed on a standard system equipped with a xenon lamp (Oriel 66902, 300W), a monochromator (Newport 66902), a Si detector (Oriel 76175_71580), and a dual channel power meter (Newport 2931_C). The impedance (real and imaginary parts) of the devices were characterized by an impedance analyzer (HP 4294) under different bias voltages.

Supporting Information

Supporting Information is available from the Wiley Online Library or from the author.

Acknowledgements

Conflict of Interest

The authors declare no conflict of interest.

References

[1]   G. Li, R. Zhu, Y. Yang, *Nat. Photonics* **2012**, 6, 153.

[2]   J. You, L. Dou, K. Yoshimura, T. Kato, K. Ohya, T. Moriarty, K. Emery, C.-C. Chen, J. Gao, G. Li, Y. Yang, *Nat. Commun.* **2013**, 4, 1446.

[3]   Z. Liu, J. Li, F. Yan, *Adv. Mater.* **2013**, 25, 4296.

[4]   G. Yu, J. Gao, J. C. Hummelen, F. Wudl, A. J. Heeger, *Science* **1995**, 270, 1789.

[5]   L. Dou, J. You, Z. Hong, Z. Xu, G. Li, R. A. Street, Y. Yang, *Adv. Mater.* **2013**, 25, 6642.

[6]   J. C. Hummelen, B. W. Knight, F. LePeq, F. Wudl, J. Yao, C. L. Wilkins, *J. Org. Chem.* **1995**, 60, 532.

[7]   F. E. Ala'a, J.-P. Sun, I. G. Hill, G. C. Welch, *J. Mater. Chem. A* **2014**, 2, 1201.

[8]   Y. Lin, X. Zhan, *Mate. Horiz.* **2014**, 1, 470.

[9]   J. Roncali, P. Leriche, A. Cravino, *Adv. Mater.* **2007**, 19, 2045.

[10]   H. Lin, S. Chen, Z. Li, J. Y. L. Lai, G. Yang, T. McAfee, K. Jiang, Y. Li, Y. Liu, H. Hu, J. Zhao, W. Ma, H. Ade, H. Yan, *Adv. Mater.* **2015**, 27, 7299.

[11]   Y. Zang, C. Z. Li, C. C. Chueh, S. T. Williams, W. Jiang, Z. H. Wang, J. S. Yu, A. K. Y. Jen, *Adv. Mater.* **2014**, 26, 5708.

[12]   Y. Zhong, M. T. Trinh, R. Chen, W. Wang, P. P. Khlyabich, B. Kumar, Q. Xu, C.-Y. Nam, M. Y. Sfeir, C. Black, M. L. Steigerwald, Y.-L. Loo, S. Xiao, F. Ng, X. Y. Zhu, C. Nuckolls, *J. Am. Chem. Soc.* **2014**, 136, 15215.

[13]   Y. H. Liu, C. Mu, K. Jiang, J. B. Zhao, Y. K. Li, L. Zhang, Z. K. Li, J. Y. L. Lai, H. W.

Hu, T. X. Ma, R. R. Hu, D. M. Yu, X. H. Huang, B. Z. Tang, H. Yan, *Adv. Mater.* **2015**, 27, 1015.

[14]   K. Cnops, B. P. Rand, D. Cheyns, B. Verreet, M. A. Empl, P. Heremans, *Nat. Commun.* **2014**, 5, 3406.

[15]   J. Zhao, Y. Li, H. Lin, Y. Liu, K. Jiang, C. Mu, T. Ma, J. Y. L. Lai, H. Hu, D. Yu, *Energy Environ. Sci.* **2015**, 8, 520.

[16]   J. Hou, O. Inganäs, R. H. Friend, F. Gao, *Nat. Mater.* **2018**, 17, 119.

[17]   P. Cheng, G. Li, X. Zhan, Y. Yang, *Nat. Photonics* **2018**, 12, 131.

[18]   J. Wang, X. Zhan, *Trends Chem.* **2019**, 1, 869.

[19]   C. Yan, S. Barlow, Z. Wang, H. Yan, A. K. Y. Jen, S. R. Marder, X. Zhan, *Nat. Rev. Mater.* **2018**, 3, 18003.

[20]   Y. Lin, J. Wang, Z.-G. Zhang, H. Bai, Y. Li, D. Zhu, X. Zhan, *Adv. Mater.* **2015**, 27, 1170.

[21]   W. Zhao, D. Qian, S. Zhang, S. Li, O. Inganäs, F. Gao, J. Hou, *Adv. Mater.* **2016**, 28, 4734.

[22]   G. Zhang, K. Zhang, Q. Yin, X.-F. Jiang, Z. Wang, J. Xin, W. Ma, H. Yan, F. Huang, Y. Cao, *J. Am. Chem. Soc.* **2017**, 139, 2387.

[23]   J. Yuan, Y. Zhang, L. Zhou, G. Zhang, H.-L. Yip, T.-K. Lau, X. Lu, C. Zhu, H. Peng, P. A. Johnson, M. Leclerc, Y. Cao, J. Ulanski, Y. Li, Y. Zou, *Joule* **2019**, 3, 1140.

[24]   S. Liu, C. Li, X. Xu, P. You, N. Wang, J. Wang, Q. Miao, F. Yan, *J. Mater. Chem. A* **2019**, 7, 12740.

[25]   S. Liu, R. Jiang, P. You, X. Zhu, J. Wang, F. Yan, *Energy Environ. Sci.* **2016**, 9, 898.

[26]   S.-W. Baek, G. Park, J. Noh, C. Cho, C.-H. Lee, M.-K. Seo, H. Song, J.-Y. Lee, *ACS Nano* **2014**, 8, 3302.

[27]   H. Choi, S.-J. Ko, Y. Choi, P. Joo, T. Kim, B. R. Lee, J.-W. Jung, H. J. Choi, M. Cha, J.-R. Jeong, I.-W. Hwang, M. H. Song, B.-S. Kim, J. Y. Kim, *Nat. Photonics* **2013**, 7,

732.

[28]   S. Liu, Y. Hou, W. Xie, S. Schlücker, F. Yan, D. Y. Lei, *Small* **2018**, 14, 1800870.

[29]   S. Liu, S. Lin, P. You, C. Surya, S. P. Lau, F. Yan, *Angew. Chem.-Int. Edit.* **2017**, 56, 13717.

[30]   K.-H. Tu, S.-S. Li, W.-C. Li, D.-Y. Wang, J.-R. Yang, C.-W. Chen, *Energy Environ. Sci.* **2011**, 4, 3521.

[31]   S.-S. Li, K.-H. Tu, C.-C. Lin, C.-W. Chen, M. Chhowalla, *ACS Nano* **2010**, 4, 3169.

[32]   Z. Liu, J. Li, Z.-H. Sun, G. Tai, S.-P. Lau, F. Yan, *ACS Nano* **2012**, 6, 810.

[33]   Z. Liu, P. You, S. Liu, F. Yan, *ACS Nano* **2015**, 9, 12026.

[34]   H. Ling, S. Liu, Z. Zheng, F. Yan, *Small Methods* **2018**, 2, 1800070.

[35]   S. Liu, P. You, J. Li, J. Li, C.-S. Lee, B. S. Ong, C. Surya, F. Yan, *Energy Environ. Sci.* **2015**, 8, 1463.

[36]   S. H. Lin, S. H. Liu, Z. B. Yang, Y. Y. Li, T. W. Ng, Z. Q. Xu, Q. L. Bao, J. H. Hao, C. S. Lee, C. Surya, F. Yan, S. P. Lau, *Adv. Funct. Mater.* **2016**, 26, 864.

[37]   Y. Huang, W. Wen, S. Mukherjee, H. Ade, E. J. Kramer, G. C. Bazan, *Adv. Mater.* **2014**, 26, 4168.

[38]   C. McDowell, M. Abdelsamie, K. Zhao, D. M. Smilgies, G. C. Bazan, A. Amassian, *Advanced Energy Materials* **2015**, 5, 1501121.

[39]   R. M. R. Rodrigues, Q. Ferreira, A. Charas, J. Morgado, *Materials* **2014**, 7, 8.

[40]   J. Bisquert, *J. Phys. Chem. B* **2002**, 106, 325.

[41]   G. Lu, J. Blakesley, S. Himmelberger, P. Pingel, J. Frisch, I. Lieberwirth, I. Salzmann, M. Oehzelt, R. Di Pietro, A. Salleo, N. Koch, D. Neher, *Nat. Commun.* **2013**, 4, 1588.

[42]   S. H. Wang, S. Fabiano, S. Himmelberger, S. Puzinas, X. Crispin, A. Salleo, M. Berggren, *Proc. Natl. Acad. Sci. USA* **2015**, 112, 10599.

[43]   J. Kang, N. Shin, D. Y. Jang, V. M. Prabhu, D. Y. Yoon, *J. Am. Chem. Soc.* **2008**, 130, 12273.

[44] G. Lu, H. Tang, Y. Huan, S. Li, L. Li, Y. Wang, X. Yang, *Adv. Funct. Mater.* **2010**, 20, 1714.

[45] M. Wang, Z. Wang, W. Ma, S.-C. Chen, Q. Zheng, *Adv. Electron. Mater.* **2016**, 2, 1600340.

[46] W. Ma, G. Yang, K. Jiang, J. H. Carpenter, Y. Wu, X. Meng, T. McAfee, J. Zhao, C. Zhu, C. Wang, H. Ade, H. Yan, *Adv. Energy Mater.* **2015**, 5, 1501400.

[47] M. Wang, D. Cai, Z. Yin, S.-C. Chen, C.-F. Du, Q. Zheng, *Adv. Mater.* **2016**, 28, 3359.

[48] J. Rieger, *J. Therm. Anal.* **1996**, 46, 965.

[49] C. W. Nies, G. L. Messing, *J. Am. Ceram. Soc.* **1984**, 67, 301.

[50] D. Fragiadakis, P. Pissis, *J. Non-Cryst. Solids* **2007**, 353, 4344.

Polystyrene is added into PBDB-T:ITIC active layers of organic solar cells, leading to a PCE enhancement up to 16% relative to the control device. Other insulating polymers can also improve the performance of the OSCs for different levels dependent on the polymer side chain size. This work provides a guideline for the selection of polymer additives in OSCs.

Keyword: Solar cells, Insulating polymer, Non-fullerene, Additive, Glass transition temperature

Meng Wang, Shenghua Liu, Peng You, Naixiang Wang, Guanqi Tang, Qian Miao and Feng YAN*

Insulating Polymers for Enhancing the Efficiency of Non-Fullerene Solar Cells
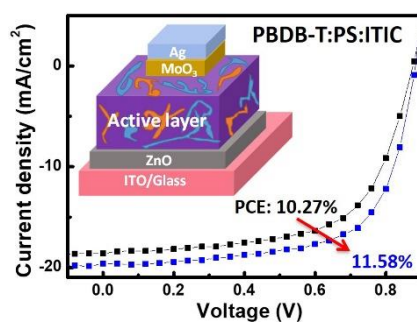
Supporting Information

Insulating polymers for enhancing the efficiency of non-fullerene organic solar cells

*Meng Wang, Shenghua Liu, Peng You, Naixiang Wang, Guanqi Tang, Qian Miao and Feng YAN**

Fabrication and characterization of hole-only and electron-only devices

In order to further estimate the hole mobilities of active layer, we also prepared hole-only devices (ITO/PEDOT:PSS/active layer/Au) and electron-only devices (ITO/ZnO/active layer/Al). The hole-only and electron-only devices were fabricated following the same procedures as those for the OSCs except that the top electrode were changed to 60 nm Au or 100 nm Al, respectively. The current-voltage curves of devices were measured by a keithley 4200A-SCS semiconductor parameter analyser in glove box. The thicknesses of the blended films were estimated by a surface profilometer. With the space charge limited current (SCLC) model, the hole mobilities were estimated by the following equation:[1]

$$J = \frac{9}{8}\varepsilon_r\varepsilon_0\mu\frac{V^2}{L^3}$$

where J is the current, ε_r is the dielectric constant of the polymer (assumed to be 3), ε_0 is the permittivity of free space (8.85×10^{-12} F m^{-1}), μ is the carrier mobility, V is the voltage drop across the device ($V = V_{appl} - V_a - V_{bi}$, where V_{appl} is the applied voltage to the device, V_a is the voltage drop due to contact resistance and series resistance across the electrodes, and V_{bi} is the built-in voltage due to the difference in work function of the two electrodes), and L is the film thickness of the active layer.
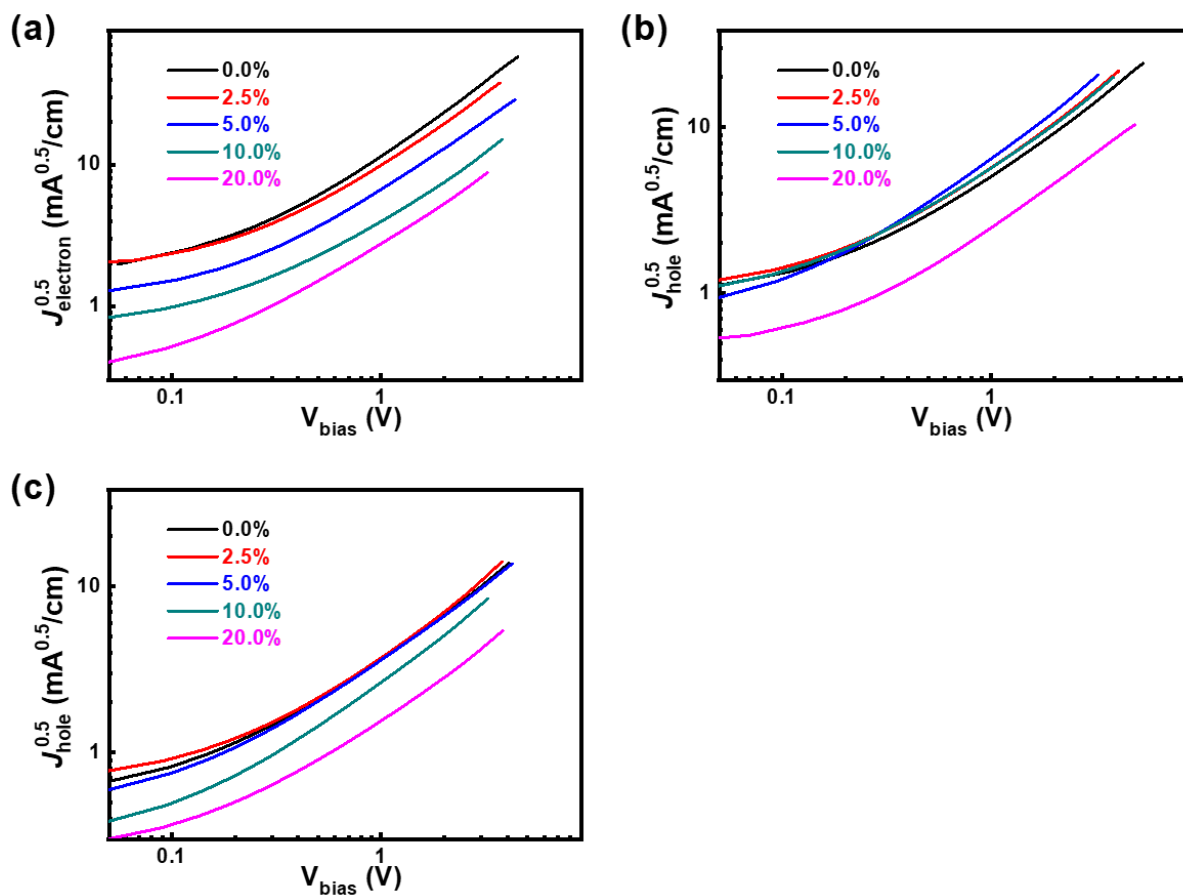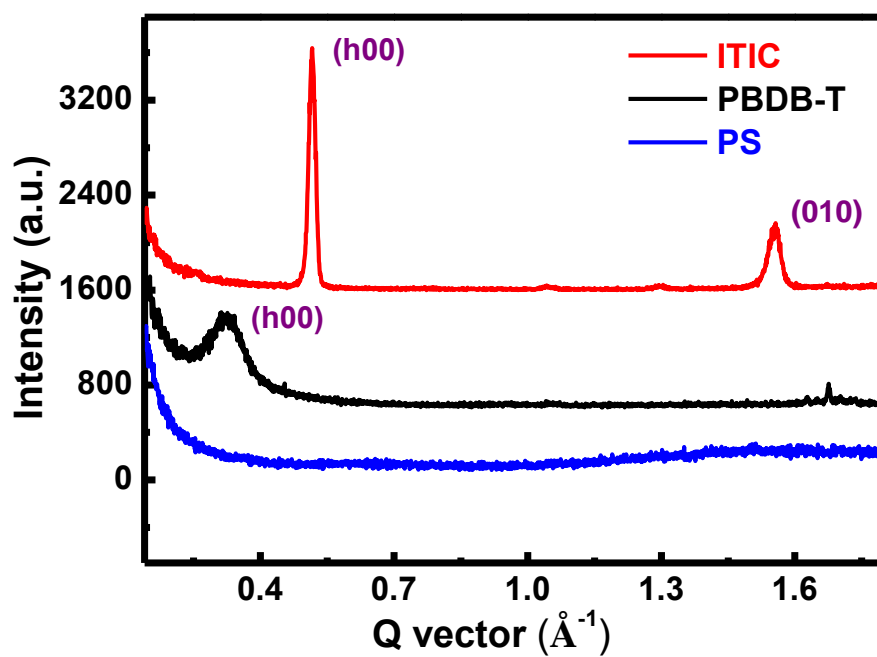
Figures
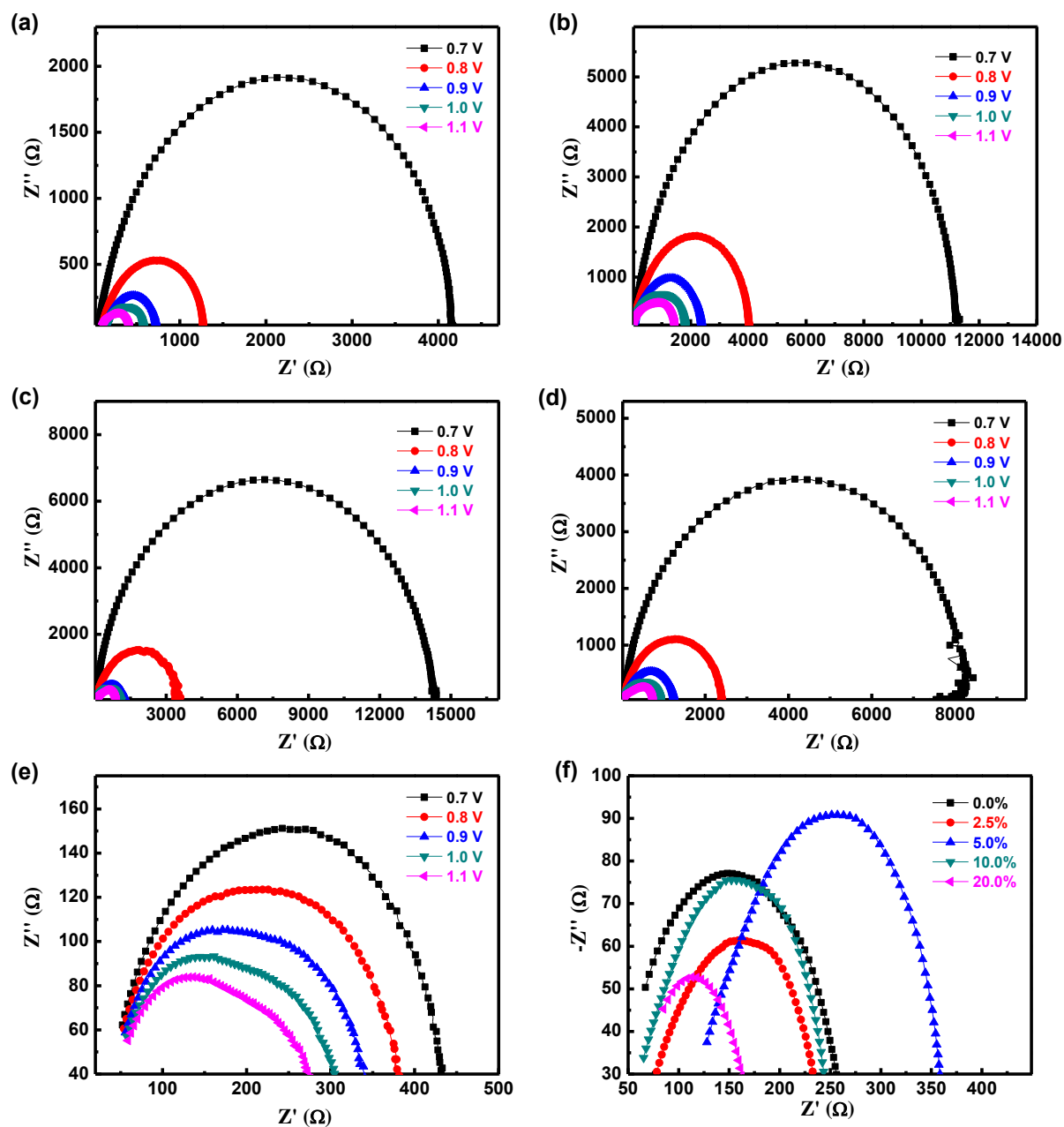
Figure S1. Impedance spectra of the conventional OSCs based on PBDB-T:ITIC with (a) 0.0%, (b) 2.5 wt.%, (c) 5.0 wt.%, (d) 10.0 wt.%, and (e) 20.0 wt.% of PS added in PBDT-T:ITIC under different bias voltages. (f) Impedance spectra of the inverted OSCs based on PBDB-T:ITIC with various percentages of PS.
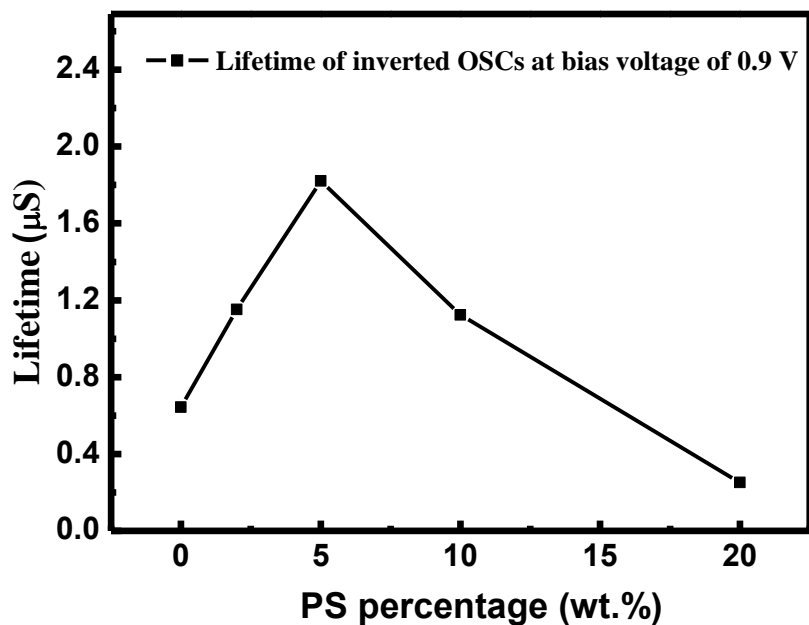
Figure S2. Carrier lifetimes of inverted OSCs with various percentages of PS at bias voltage of 0.9 V.

Figure S3. $J^{0.5} \sim V$ characteristics of (a) electron-only and (b) hole-only devices based on PBDB-T:ITIC blends with various percentages of PS. (c) $J^{0.5} \sim V$ curves of hole-only devices based on PBDB-T blended with different percentages of PS.

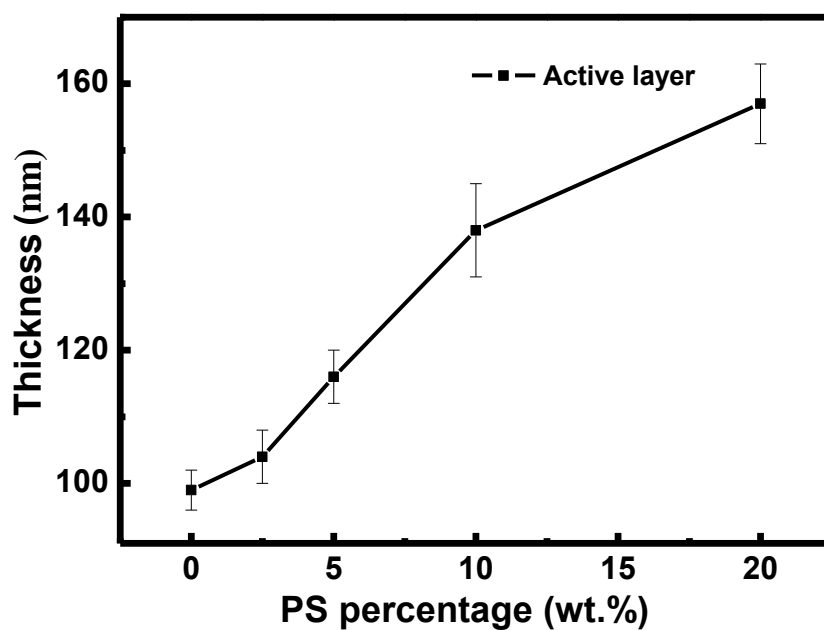**Figure S4.** The GIXD out-of-plane diffraction profiles of an ITIC film, a PBDB-T film, and a PS film.
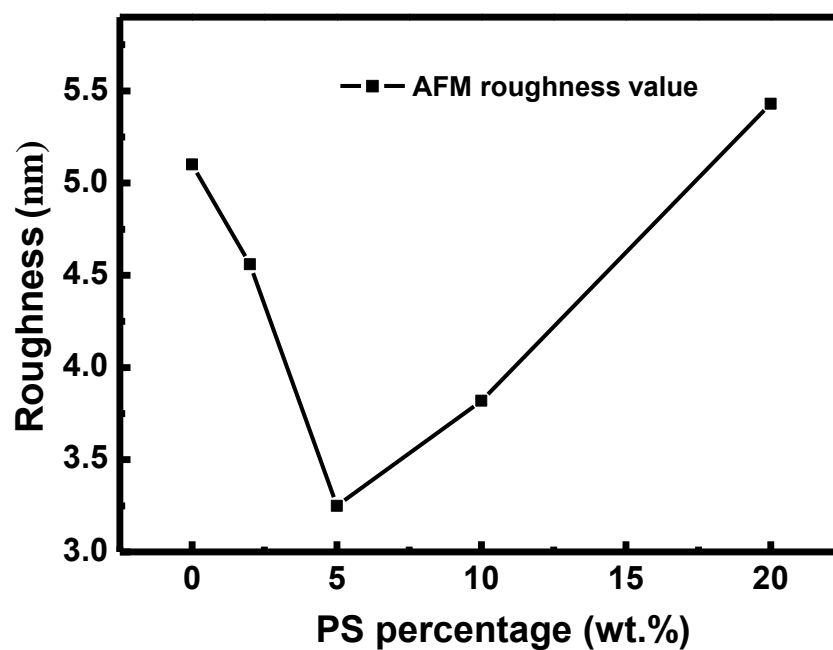
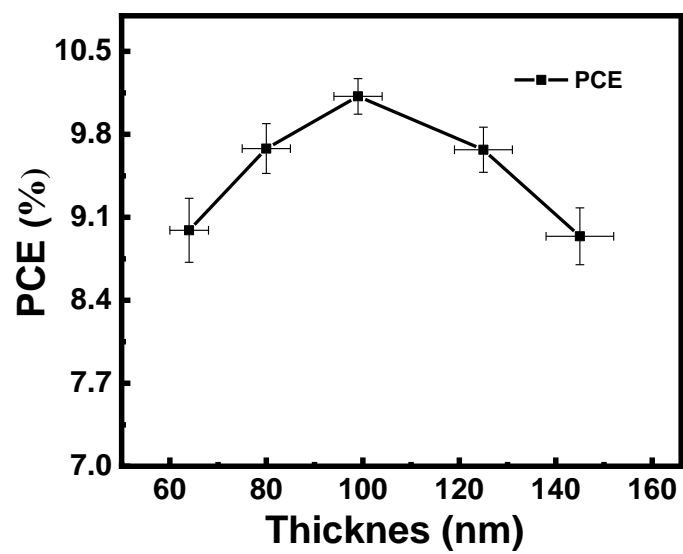**Figure S5.** Roughness of PBDB-T:ITIC film incorporated with different percentages of PS.

Figure S6. Thickness of PBDB-T:ITIC films incorporated with 0.0%, 2.5 wt.%, 5.0 wt.%, 10.0 wt.%, or 20.0 wt.% PS, respectively.
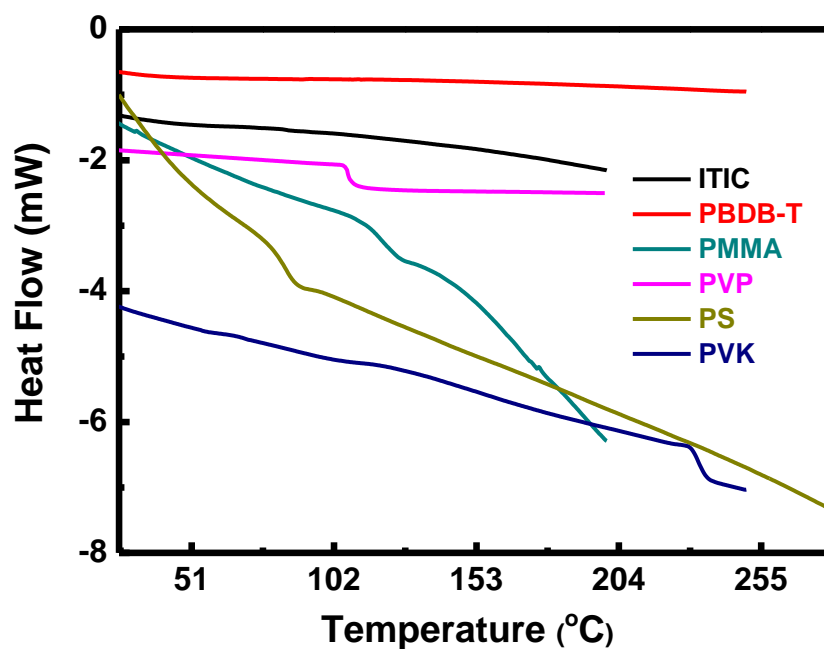
Figure S7. DSC traces of the polymers with a heating rate of 20 °C/min under nitrogen.

Figure S8. Photovoltaic properties of inverted OSCs based on PBDB-T:ITIC blends with different active layer thickness.

Tables:

Table S1. Photovoltaic properties of inverted OSCs based on PBDB-T:PS:ITIC blends with thermal annealing under various temperatures

Temperature (°C)	PS ratio[a] (wt.%)	V_{oc} (V)	J_{sc} (mA/cm^2)	FF (%)	PCE (%)	Enhancement[b] (%)
	0.0	0.88	17.67	61.81	9.72 (9.65±0.08)	0
	2.5	0.88	18.16	60.13	9.67 (9.60±0.07)	-0.52±0.62
70	5.0	0.88	18.17	59.07	9.51 (9.45±0.06)	-2.07±0.73
	10.0	0.88	18.11	58.68	9.50 (9.38±0.12)	-2.80±1.24
	20.0	0.88	18.18	56.84	9.22 (9.16±0.06)	-5.08±0.62
	0.0	0.88	18.39	61.96	10.01 (9.89±0.12)	0
	2.5	0.88	18.51	61.77	10.08 (9.96±0.13)	0.71±1.31
90	5.0	0.88	18.02	64.05	10.12 (10.02±0.10)	1.31±1.0
	10.0	0.88	17.71	61.31	10.03 (9.95±0.08)	0.61±0.81
	20.0	0.88	18.78	59.10	9.83 (9.75±0.14)	-1.42±1.42
	0.0	0.88	18.15	62.75	10.13 (10.01±0.12)	0
	2.5	0.88	18.15	64.68	10.36 (10.29±0.07)	2.80±0.70
110	5.0	0.88	18.89	66.46	11.04 (10.90±0.14)	8.89±1.40
	10.0	0.88	18.13	66.56	10.62 (10.54±0.08)	5.29±0.80
	20.0	0.88	18.21	62.74	10.35 (10.16±0.19)	1.50±1.90

[a] PS percentage was relative to the PBDB-T (w/w). [b] Enhancement was calculated according to the average PCE.

Table S2. Photovoltaic properties of conventional OSCs based on PTB7:PS:PC$_{71}$BM blends

Percentage[a] (wt.%)	V_{oc} (V)	J_{sc} (mA/cm^2)	FF (%)	PCE (%)	Enhancement[b] (%)
0.0%	0.72	16.67	66.40	7.96 (7.86±0.10)	0
2.5%	0.72	16.15	66.70	7.75 (7.68±0.12)	-2
5.0%	0.76	15.99	63.20	7.68 (7.61±0.07)	-3
10.0%	0.76	14.72	64.50	7.22 (7.20±0.03)	-8
20.0%	0.76	15.01	58.40	6.66 (6.50±0.08)	-17

[a] PS percentage was relative to the PTBT (w/w). [b] Enhancement was calculated according to the average PCE.

Table S3. Photovoltaic properties of inverted OSCs based on PBDB-T:ITIC incorporated with various percentages of insulating polymers

Insulator	M_w (KDa)	T_g (°C)	Percentage [a] (wt.%)	V_{oc} (V)	J_{sc} (mA/cm²)	FF (%)	PCE (%)	Enhancement [b] (%)
None	-	-	0.0	0.88	18.62	62.89	10.27 (10.12±0.15)	0
PS	35	84	2.5	0.88	19.51	64.83	11.14 (11.02±0.12)	8.89±1.19
			5.0	0.88	19.64	67.00	11.58 (11.42±0.16)	12.85±1.58
			10.0	0.88	18.75	66.90	11.05 (10.92±0.13)	7.91±1.28
			20.0	0.88	19.09	62.40	10.47 (10.42±0.05)	2.96±0.49
PEG	1	17	2.5	0.87	19.32	61.74	10.42 (10.32±0.10)	1.98±0.99
			5.0	0.88	19.32	61.36	10.41 (10.31±0.10)	1.88±0.99
			10.0	0.87	19.16	60.55	10.10 (10.02±0.08)	-0.99±0.79
			20.0	0.87	19.75	58.21	9.98 (9.72±0.26)	-3.95±2.57
PDMS	63	-113	2.5	0.88	19.28	61.72	10.44 (10.33±0.11)	2.08±1.09
			5.0	0.88	19.47	63.91	10.92 (10.83±0.09)	7.02±0.89
			10.0	0.87	19.47	60.94	10.36 (10.22±0.14)	0.99±1.38
			20.0	0.86	19.46	60.08	10.05 (9.92±0.13)	-1.98±1.28
PMMA	120	107	2.5	0.89	19.14	62.29	10.58 (10.41±0.17)	2.87±1.68
			5.0	0.87	19.87	64.70	11.14 (11.08±0.06)	9.49±0.59
			10.0	0.87	19.67	62.41	10.74 (10.66±0.08)	5.34±0.79
			20.0	0.86	19.39	57.80	9.59 (9.47±0.12)	-6.42±1.19
PVP	40	106	2.5	0.87	19.50	66.49	11.33 (11.10±0.23)	9.68±2.27
			5.0	0.87	19.15	62.66	10.39 (10.25±0.11)	1.28±1.09
			10.0	0.85	19.71	60.43	10.09 (9.93±0.16)	-1.88±1.58
			20.0	0.81	19.13	57.35	8.91 (8.84±0.07)	-12.65±0.69
PVK	90	226	2.5	0.85	19.32	59.43	9.79 (9.69±0.13)	-4.25±1.28
			5.0	0.86	19.14	58.02	9.50 (9.35±0.15)	-7.61±1.48
			10.0	0.87	17.27	60.20	9.04 (8.82±0.22)	-12.85±2.17

| | 20.0 | 0.84 | 15.39 | 57.51 | 7.41 (7.28±0.23) | -28.06±2.27 |

[a] Insulator percentage was relative to the PBDB-T (w/w). [b] Enhancement was calculated according to the average PCE.

References

1. S. Albrecht, S. Janietz, W. Schindler, J. Frisch, J. Kurpiers, J. Kniepert, S. Inal, P. Pingel, K. Fostiropoulos, N. Koch, and D. Neher, *J. Am. Chem. Soc.*, **2012**, *134*, 14932.